Chapter 7

Selection and Analysis of $\gamma\gamma$ Events

7.1 Initial Data Selection

The $\gamma\gamma$ events analyzed for this dissertation are collected in the "gold gg" data stream. The requirements for this trigger subset are loose - so that $\gamma\gamma$ events are accepted with 100% efficiency. As a result, the vast majority of the initial "gold gg" data sample are $\pi^0\pi^0$, $\pi\eta$ and $\eta\eta$ events, which constitute the main sources of background to the $\gamma\gamma$ final state. This is illustrated in Fig. 7.1, in which we have plotted for each "gold gg" event the invariant mass combinations between each of the two largest energy clusters (γ_1 and γ_2) and additional clusters in the calorimeter. $\pi^0\pi^0$, $\pi^0\eta$ and $\eta\eta$ events are all readily apparent. We describe below the cuts which we use to extract a final selection of $\gamma\gamma$ candidate events from this background.

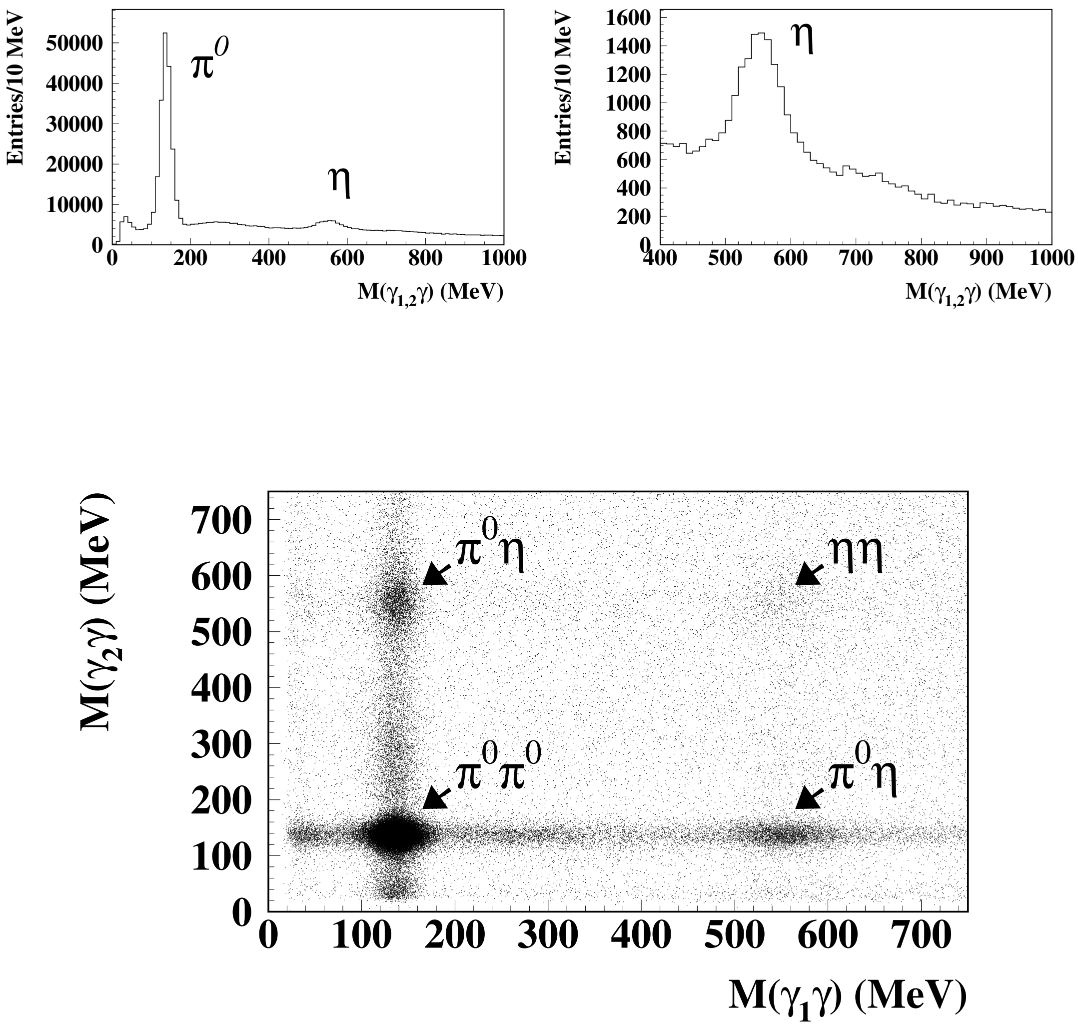

Figure 7.1: Invariant mass combinations calculated with each γ candidate and untimed extra clusters in the CCAL, showing π^0 (upper left), η (upper right), and (bottom) the dominance of $\pi^0\pi^0$ events in the "gold gg" trigger sample.

7.2 $\gamma\gamma$ Event Selection Criteria

Cuts are made using the following information:

- Cluster time
- Invariant mass between γ candidate cluster and "extra" CCAL clusters
- Event kinematics (χ^2 probability for 4C kinematic fit or $\Delta\phi$ and $\Delta\theta$)
- Polar angle θ of γ candidates
- Charged Hodoscope ($H1$, $H2'$) pulse height

7.2.1 Cluster Time Cut

In E835 the instantaneous luminosity was significantly increased compared to E760, and in order to be able to retain real events which are contaminated with additional interactions in the same CCAL FERA gate, each CCAL block was outfitted with TDCs (see Sec. 4.4.3). The effect of this timing capability is two-fold. First, it allows us to remove a large part of the $\pi^0\pi^0$, etc. events from the trigger sample very efficiently by cutting on the number of in-time clusters. Second, it allows us to retain the $\gamma\gamma$ events which contain "extra" CCAL clusters associated with "out-of-time" interactions.

Definition of Cluster Time

The "time" of a cluster is defined as the TDC value of the largest energy block in the cluster which has a TDC hit. Most of the time, this is the central block (i.e. the

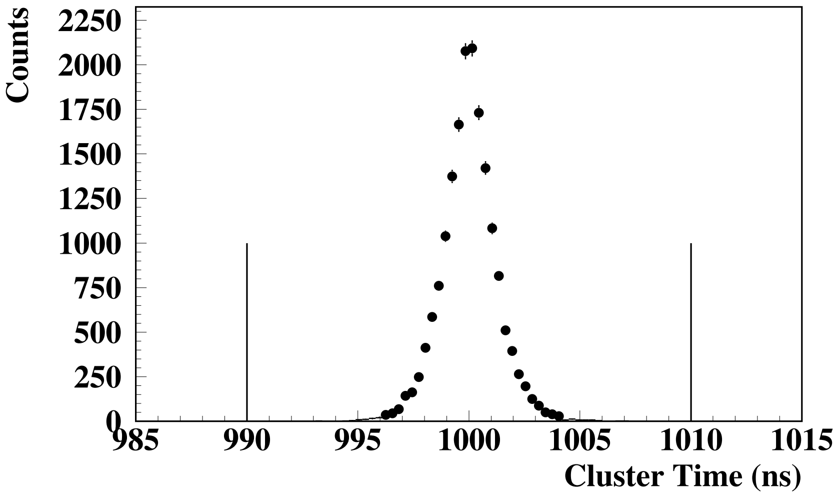

Figure 7.2: Cluster times for the two large-energy clusters in a sample of clean $\pi^0\pi^0$ events, taken at $\sqrt{s} = 3576$ MeV. The FWHM of this distribution is ~ 5.8 ns. The "in-time" window is indicated by the vertical lines.

largest energy block), but occasionally that block will have no TDC hit. In these cases, the cluster time comes from the second-largest energy block in the cluster. If no block in the cluster has a TDC hit, then its time is recorded as 0, and the cluster is referred to as an "untimed" cluster. We define a cluster as "in-time" if its TDC signal lies within ± 10 ns of the mean event time of 1000 ns. If a cluster's time is non-zero, but outside this 20 ns window, it is called "out-of-time".

The time for each of the two large-energy clusters in a set of clean $\pi^0\pi^0$ events (selected by requiring 4 CCAL clusters exactly, and two reconstructed π^0 masses - 100 to 170 MeV) is shown in Fig. 7.2. The vertical lines in the figure define the 20ns "in-time" window.

Effect of Timing

As mentioned earlier, the capability of timing CCAL clusters is helpful in two ways: we are able to reject events with more than two in-time clusters, and we are able to retain true $\gamma\gamma$ events which contain additional CCAL clusters which arise from noise or out-of-time interactions. Figs. 7.3 and 7.4 illustrate the effect of having this timing capability.

In Fig. 7.3 we show the number of CCAL clusters for events which pass all cuts discussed in this chapter, except the timing cut. As expected, most events have just two clusters (334/661). Fig. 7.4 shows the same for events which pass all cuts, including the timing (334/434 have just two clusters). If we had no timing capability, we would have the choice in Fig. 7.3 of accepting events which have only 2 CCAL clusters (334), or accepting events irrespective of the number of CCAL clusters they contain (661). In the former case, we would lose many good $\gamma\gamma$ events ($434 - 334 = 100$) due to the presence of extra clusters in the CCAL. In the latter case, we would be accepting accepting a larger amount of background ($661 - 434 = 227$)

Description of the cut

We accept only events which contain only two in-time clusters in the CCAL. These two must be the two largest energy clusters (i.e., the photon candidates). Any number of additional clusters may be present in the CCAL, but no cluster besides the γ candidates may have a time which is in the 20 ns window from 990 ns to 1010 ns. (See Fig. 7.2)

Since we only allow two on-time clusters, the timing cut removes a large per-

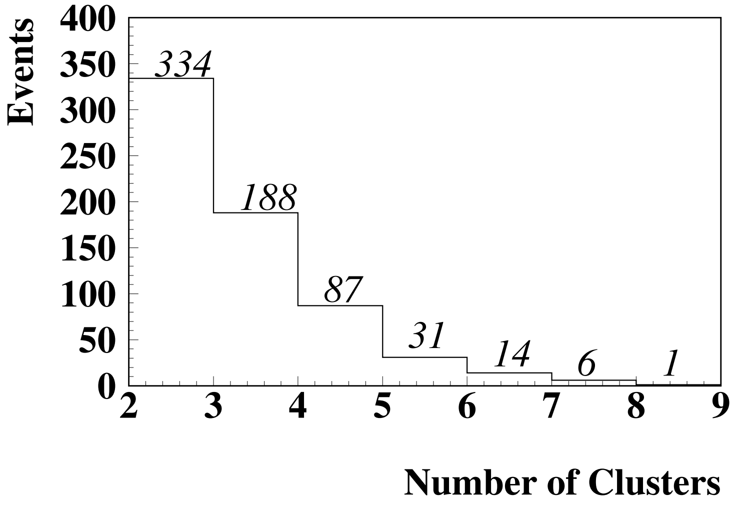

Figure 7.3: Number of CCAL clusters for events (taken from four runs near the η_c peak) which pass all the cuts discussed in this chapter, except the timing cut.

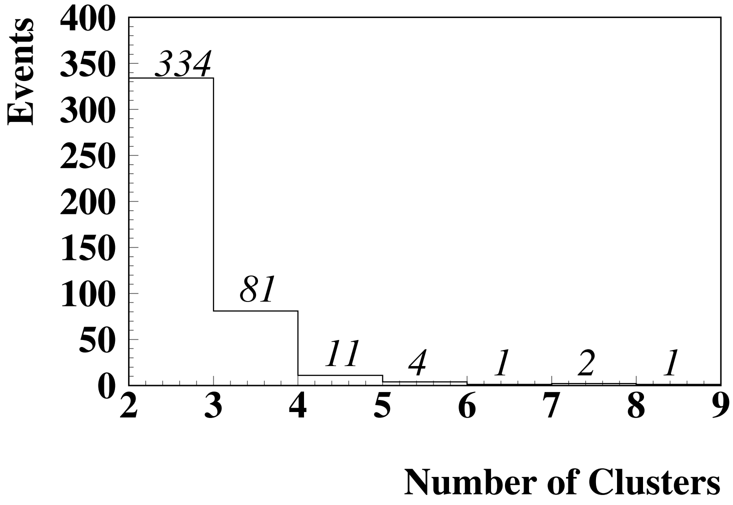

Figure 7.4: Number of CCAL clusters for events (taken from four runs near the η_c peak) which pass all cuts discussed in this chapter.

Table 7.1: $\pi^0\pi^0(\pi^0\gamma)$ events with exactly 4(3) CCAL clusters, with $N_{on-time}$ having an in-time TDC signal. Note the high rejection factor for $\pi^0\pi^0$ and $\pi^0\gamma$ events if $N_{in-time} = 2$ is used.

Region	$\pi^0\pi^0$ Events	$N_{in-time}$ 4	3	2	Rejection Factor	$\pi^0\gamma$ Events	$N_{in-time}$ 3	2	Rejection Factor
η_c	12538	11846	683	9	0.9993	16470	16127	343	0.9792
$^1P_1$	5076	4815	260	1	0.9998	6509	6346	163	0.9750
η_c'	2563	2435	127	1	0.9996	3120	3029	91	0.9708

centage of fully-accepted $\pi^0\gamma$ and $\pi^0\pi^0$ events. An examination of the number of on-time clusters for a clean selection of $\pi^0\gamma$ and $\pi^0\pi^0$ events demonstrates this fact.

For this study, $\pi^0\pi^0$ events were chosen by requiring that there be precisely four clusters in CCAL and that two invariant masses $M(\gamma_{1,2}\gamma)$ in the range 115-155 MeV be found. $\pi^0\gamma$ events were selected in a similar way, requiring one $M(\gamma_{1,2}\gamma)$ combination in the same range, and exactly three CCAL clusters. The number of events having $N_{in-time}$ in-time clusters for each of these cases can be found in Table 7.1, for data taken in the vicinity of η_c and χ_2, and in the search region for η_c'. We note that when the $N_{in-time} = 2$ cut alone is applied, less than $\sim 0.07\%$ of the $\pi^0\pi^0$ events, and less than $\sim 2.5\%$ of the $\pi^0\gamma$ events, are retained. As an aside, we note that $\sim 5\%$ of the $\pi^0\pi^0$ events have only 3 in-time clusters and that $\sim 2.5\%$ of the $\pi^0\gamma$ events have only two in-time clusters.

The $N_{in-time} = 2$ cut will be inefficient for selecting $\gamma\gamma$ final states only if additional interactions occurring within ± 10 ns of the trigger interaction cause extra in-time hits, or if random noise produces a cluster with an in-time TDC hit. The inefficiency induced by each of these situations may be dependent on the instantaneous luminosity, and therefore the efficiency of the timing cut has been studied in conjunction with other cuts which are expected to be luminosity dependent. The study of the combined efficiency of such cuts is described in Sec. 7.2.4.

7.2.2 Invariant mass between γ candidate cluster and "extra" clusters

After applying the $N_{in-time} = 2$ cut, remaining events contain either the 2 in-time clusters alone, or in addition, some number of out-of-time or untimed clusters. Lower energy clusters (below 50 MeV or so) have a $\gtrsim 20\%$ chance of being untimed, as illustrated in Fig. 7.5. Because of this drop in timing efficiency with decreasing cluster energy, it is possible that a real $\pi^0\gamma$ event, for instance, may be observed in the CCAL as a pair of γ candidates accompanied by a third cluster which is either untimed or out-of-time. Such events are removed as described below.

We calculate invariant masses $M(\gamma_{1,2}\gamma)$ between all untimed or out-of-time clusters and each of the γ candidates, γ_1 and γ_2. We reject events which have one or more invariant mass combinations in the π^0 mass range $100 \leq M(\gamma_{1,2}\gamma)(\text{MeV}) \leq 170$. The invariant mass spectrum of the pairs (γ_1, γ and γ_2, γ) is shown in Fig. 7.6, and the cut region is indicated.

In the E760 analyses of the $\gamma\gamma$ final state, [48, 49] events having a combination of $M(\gamma_{1,2}\gamma)$ near the η mass (549 MeV) were also removed. We do not make such a cut in E835, however, because the CCAL timing capability makes the cut unnecessary. While the lower energy photon from π^0 decay (in a $\pi^0\pi^0$ or $\pi^0\gamma$ event) may sometimes have a wrongly assigned time, resulting in an untimed or out-of-time cluster, in the case of η's this happens rarely, if ever. The absence of a discernible excess in the

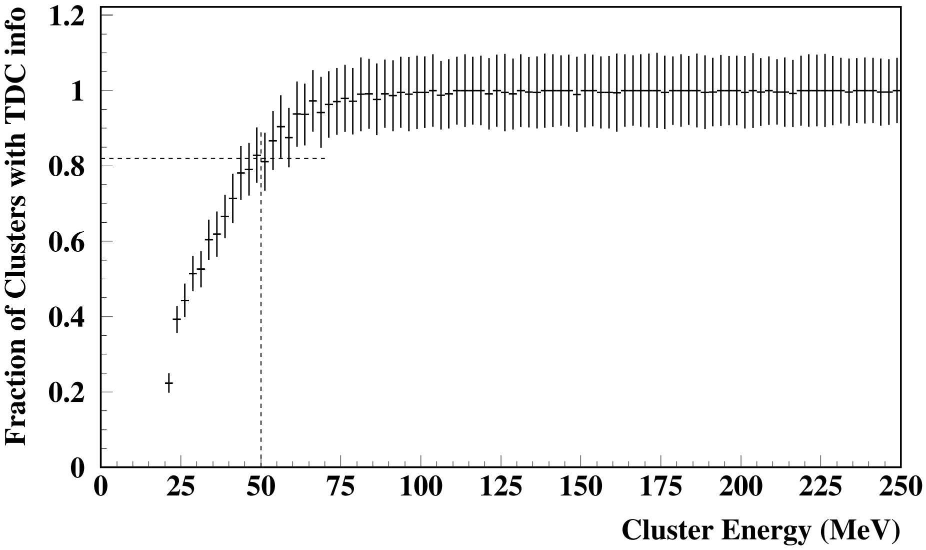

Figure 7.5: Fraction of clusters which have timing information. These clusters were chosen from $\pi^0\pi^0$ events, in which all four clusters are reconstructed in the CCAL, and therefore should in principle have in-time signals. The dashed lines indicate, *e.g.*, that $\sim 82\%$ of 50 MeV clusters have correct timing information.

$M(\gamma_{1,2}\gamma)$ spectrum near 550 MeV in Fig. 7.6, is testimony to this fact.

The efficiency of this cut has been studied in combination with other cuts which have a possible luminosity dependence, and the results of that study are reported in Sec. 7.2.4.

7.2.3 Kinematic cuts

Next, the $\gamma\gamma$ candidate events are evaluated for consistency with the kinematics of $\bar{p}p \rightarrow \gamma\gamma$. We have investigated two ways of doing this. First, a 4C kinematic fit may

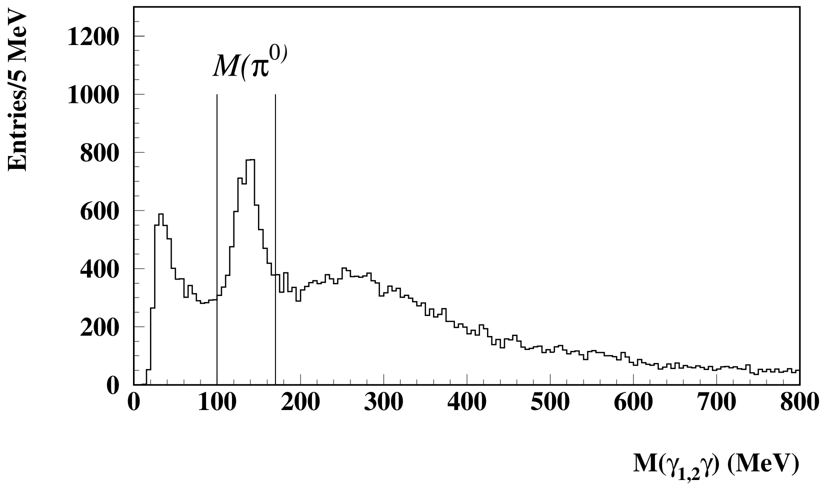

Figure 7.6: Invariant mass spectrum: $M(\gamma_{1,2}\gamma)$ between γ candidates and any untimed or out-of-time clusters in the CCAL. This spectrum was produced with data taken from runs in the η_c' region.

be performed on the two γ candidates, from which a χ^2 probability may be calculated and cut on. Second, separate cuts on the variables $\Delta\theta = (\theta_{\text{measured}} - \theta_{\text{expected}})$ and $\Delta\phi = (|\phi_1 - \phi_2| - \pi)$ may be made. In the analysis presented in this dissertation, we have chosen to use the first method, though the second method is an entirely proper alternative. We explain our choice in the following.

Cuts on χ^2 Probability: The χ^2 probability for a clean selection of $J/\psi \to e^+e^-$ events (chosen from the "gold ee" trigger set, requiring only 2 clusters in the CCAL, and pulse heights in the Čerenkov of 0.5-1.5 units for each electron candidate) is shown in Fig. 7.7. Our chosen χ^2 probability cut of 5% is indicated in the figure

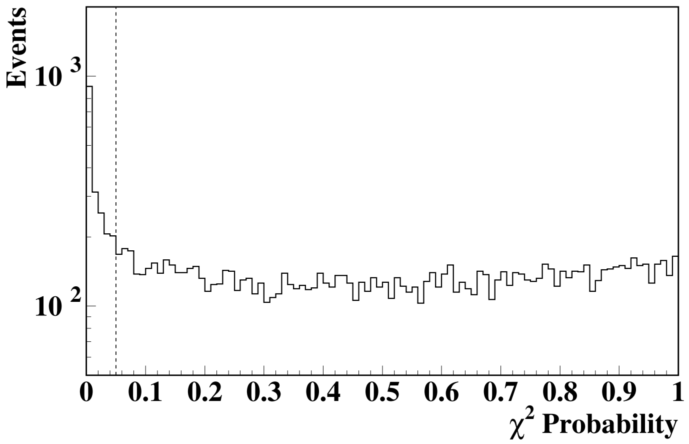

Figure 7.7: χ^2 probability for clean $J/\psi \to e^+e^-$ events. The dashed line indicates our chosen cut value of 5%.

by the dashed line. We have estimated the efficiency of this cut using the clean sample of $J/\psi \to e^+e^-$ events from our data. The efficiency for various values of the χ^2 probability cut is shown in Table 7.2.

In an effort to check the stability of this cut throughout the E835 run, we have calculated the efficiency of the cut for individual J/ψ stacks, and the result is shown in Table 7.2 as well. This efficiency appears to be quite stable throughout the run, though the last set of runs (3078-3079) indicates a possible problem. There are, however, no known problems with the CCAL or instantaneous luminosity for this set of runs. Other consistency checks of the CCAL do not exhibit this problem; so we conservatively estimate a systematic error of 1%, so that the efficiency of the cut at χ^2 probability $\leq 5\%$ as determined by the J/ψ data sample is $87.30 \pm 0.25 \pm 1.00\% = 87.3 \pm 1.03\%$.

Table 7.2: Efficiencies of various χ^2 probability cuts for $J/\psi \to e^+e^-$ events.

Probability Cut level	Efficiency (%) at J/ψ
0.5%	95.20 ± 0.16
1%	93.84 ± 0.18
5%	87.30 ± 0.25
10%	81.92 ± 0.29

Probability cut at 5%	
Runs	Efficiency (%)
824-831	87.49 ± 0.49
908-909	87.81 ± 0.49
1331-1336	87.20 ± 0.52
2285-2286	88.02 ± 0.56
3078-3079	83.82 ± 0.96

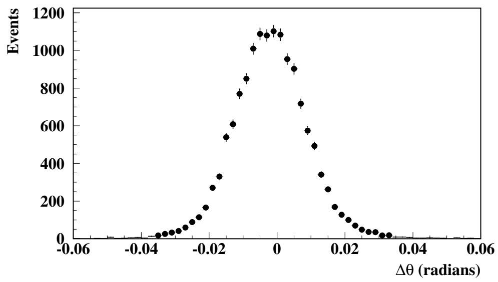

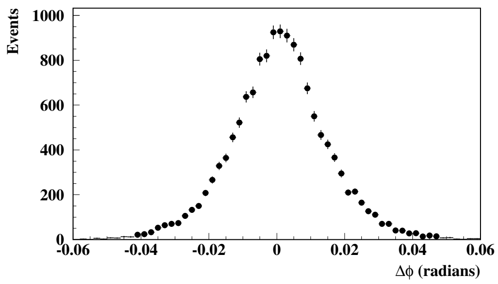

Figure 7.8: $\Delta\theta$ (left) and $\Delta\phi$ (right) distributions for clean $J/\psi \to e^+e^-$ events..

Cuts on $\Delta\theta$ and $\Delta\phi$: In an effort to determine whether a different set of cuts on two-body kinematics of the γ candidates are useful, we have studied the efficiency of cuts on $\Delta\theta$ and $\Delta\phi$. The $\Delta\theta$ and $\Delta\phi$ distributions for the set of clean J/ψ events described earlier are shown in Fig. 7.8.

The mean values of $\Delta\theta$ and $\Delta\phi$ are not zero, but change somewhat from stack to stack, or even from run to run. We therefore consider cuts which are dependent on the difference between $\Delta\theta$ ($\Delta\phi$) and the mean value, $\overline{\Delta\theta}$ ($\overline{\Delta\phi}$). We refer to these cuts as cuts on the 'rescaled' variables $\Delta_R(\theta) = |\Delta\theta - \overline{\Delta\theta}|$ and $\Delta_R(\phi) = |\Delta\phi - \overline{\Delta\phi}|$. The efficiencies for various cut values of rescaled $\Delta_R(\theta)$ and $\Delta_R(\phi)$ are given in

Table 7.3: Efficiencies of $\Delta_R(\theta)$ and $\Delta_R(\phi)$ cuts. (expressed in %)

	$\Delta_R\phi$		
$\Delta_R\theta$	0.015	0.020	0.025
0.015	62.36 ± 0.36	71.86 ± 0.34	77.33 ± 0.31
0.020	68.45 ± 0.35	78.92 ± 0.30	85.00 ± 0.27
0.025	71.00 ± 0.34	81.87 ± 0.29	88.20 ± 0.24
0.030	72.15 ± 0.33	83.23 ± 0.29	89.68 ± 0.23
	$\Delta_R\phi$		
$\Delta_R\theta$	0.027	0.030	0.035
0.015	78.87 ± 0.30	80.63 ± 0.29	82.39 ± 0.28
0.020	86.64 ± 0.25	88.63 ± 0.24	90.61 ± 0.22
0.025	89.96 ± 0.22	92.05 ± 0.20	94.10 ± 0.18
0.030	91.46 ± 0.21	93.59 ± 0.18	95.67 ± 0.15

Table 7.3

As a test for the stack-to-stack stability of this cut (to be compared with that of the χ^2 cut discussed previously), we chose values of $\Delta_R(\theta)$ and $\Delta_R(\phi)$ for which the cut efficiency is approximately the same ($\sim$ 87%) as for a χ^2 cut at 5%. One set of these values is $\Delta_R(\theta) = 0.020$ and $\Delta_R(\phi) = 0.027$. The efficiencies of this cut for each of the four J/ψ stacks considered earlier are given in Table 7.4. As is apparent from the table, this cut may be more stable from stack to stack, and its use therefore would lead to a somewhat smaller systematic error ($\sim$ 0.5%).

However, while the probability cut and the $\Delta_R(\theta), \Delta_R(\phi)$ cuts are nearly equally efficient for $\bar{p}p \to J/\psi \to e^+e^-$, their ability to reject background is not equal. We have studied the background level accepted by each cut, and find that the cut on χ^2 probability is more efficient at removing background. For example, for a set of ten $^1P_1$ stacks, where we expect no $\gamma\gamma$ signal, we have applied the two kinematic cuts to events which pass all other cuts mentioned in this chapter. Of these 'background'

Table 7.4: Efficiencies of $\Delta_R(\theta)$ cut at 0.020 and $\Delta_R(\phi)$ at 0.027 for various J/ψ runs.

Runs	Efficiency (%)
824-831	86.43 ± 0.51
908-909	87.22 ± 0.50
1331-1336	86.58 ± 0.53
2285-2288	86.36 ± 0.59
3078-3079	86.39 ± 0.89

events, the $\Delta_R(\theta)$ and $\Delta_R(\phi)$ cuts reject $\sim 60\%$ while the χ^2 probability cut rejects $\sim 70\%$.

We have also considered six other combinations of $\Delta_R(\theta)$ and $\Delta_R(\phi)$ which have approximately the same efficiency as the choice of $\Delta_R(\theta) = 0.02$ and $\Delta_R(\phi) = 0.027$ which we studied above. They all are found to have nearly the same background rejection efficiency. We have therefore decided to use the χ^2 probability cut.

7.2.4 Effect of "Noise" and Extraneous Interactions on Efficiency

As instantaneous luminosity varies, the efficiencies of several cuts mentioned above may change. The rate of interactions is proportional to instantaneous luminosity - and therefore, the occurrence of clusters in the CCAL due to interactions other than a triggered event increases as the instantaneous luminosity is increased. The rate of false neutral vetoes increases in a similar manner. Further, random noise in the CCAL and other detectors may also be stack-dependent.

The occurrence of each of these problems is best studied by using Monte Carlo $\gamma\gamma$ events superimposed with events from the random gate trigger. For each E835 stack, a Monte Carlo set of 100,000 $\gamma\gamma$ events is generated. Then, for each Monte Carlo event, CCAL and hodoscope information from a random gate event is added to the information which has been simulated by Monte Carlo. In this way, the activity of the detector, due either to random noise or additional interactions during the same FERA gate, are simulated.

By this technique it is possible to estimate the fraction of real $\gamma\gamma$ events which are removed from the data set due to

1. random noise which generates extra in-time clusters,
2. $m(\pi^0)$ combinations between the γ candidates and clusters due to random noise or out-of-time interactions, or
3. a false Neutral Veto due to noise, or a coincident charged interaction.

This study was performed for every E835 stack. The efficiencies calculated for the combination of the cuts on timing, $M(\gamma_{1,2}\gamma)$ and the χ^2 probability, and the inefficiency for the neutral veto, are shown in Fig. 7.9 as a function of the instantaneous luminosity. These data have been fitted to a line:

$$\epsilon_{LD} = (0.947 \pm 0.002) - (0.109 \pm 0.001) \times \mathcal{L}, \tag{7.1}$$

where the instantaneous luminosity $\mathcal{L}$ is expressed in units of $10^{31}\text{cm}^{-2}\ \text{sec}^{-1}$. However, in the analysis of the $\gamma\gamma$ data, we have chosen to use the individual stack-by-stack calculated efficiencies, because the fit has a large $\chi^2/d.o.f = 9.3$.

In the course this study, it was coincidentally discovered that the efficiency of the cut on χ^2 probability has a significant energy dependence. Therefore, using a

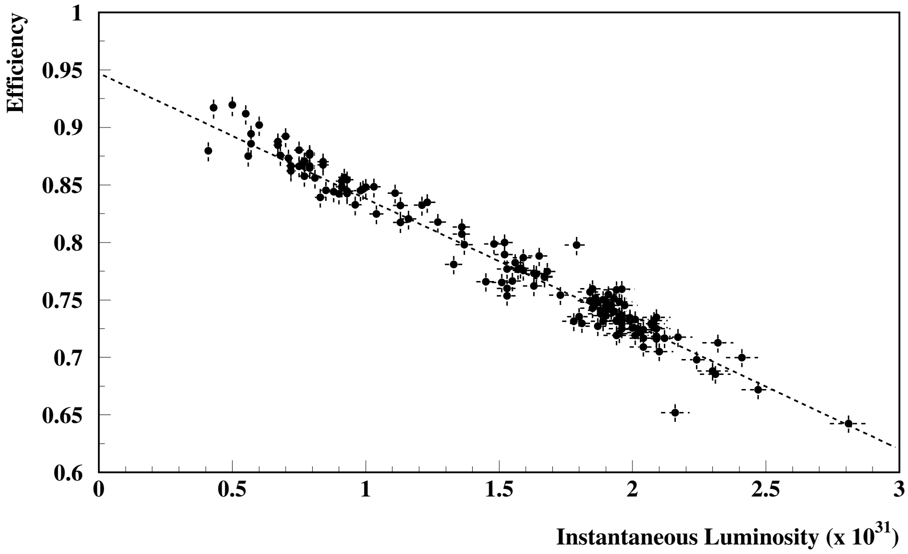

Figure 7.9: The combined efficiency of timing and $m(\pi^0)$ cuts, and of the neutral veto, plotted versus instantaneous luminosity. The horizontal error bars represent the $\pm 2.5\%$ error on the luminosity measurements. The dashed line represents the results of a fit to these data.

single value for all stacks for the efficiency of cut would be incorrect. Therefore, the efficiency of this cut has also been calculated on a stack-by-stack basis. In Fig 7.10 we show the efficiency $\epsilon(\chi^2)$ of the 5% χ^2 probability cut as a function of $\sqrt{s}$. Again, these efficiencies are applied on a stack-by-stack basis in the analysis of $\gamma\gamma$ data, because the fit has a poor $\chi^2/d.o.f$ of 6.6.

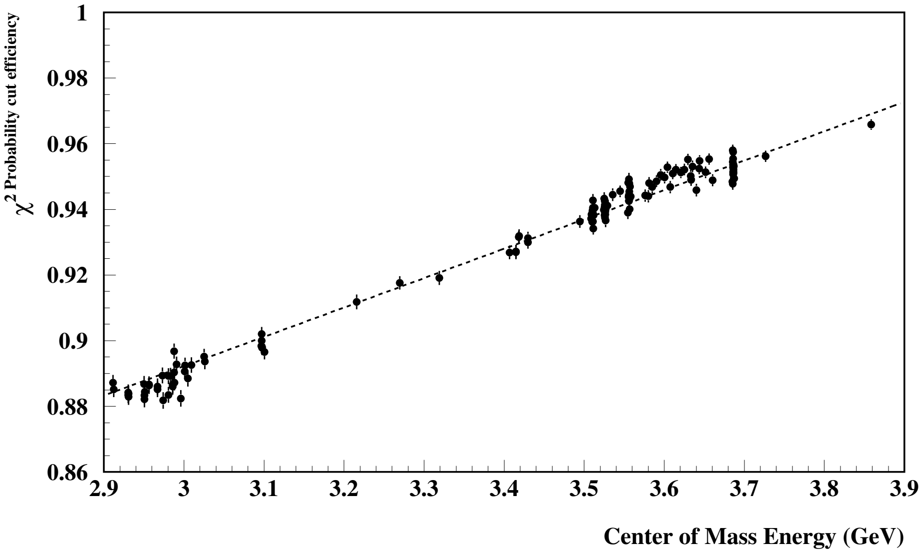

Figure 7.10: The calculated efficiency of the 5% χ^2 probability cut, as a function of center of mass energy $\sqrt{s}$, for events with $|\cos\theta^*| \leq 0.2$. The dashed line represents the results of a fit to these data.

7.2.5 Polar Angle θ of the γ candiates.

As was the case in E760, the background of $\pi^0\pi^0$ and $\pi^0\gamma$ events which feed-down into the $\gamma\gamma$ final state is large compared to the signal. [50], [51] As a result, even after the above cuts have been made, the majority of events which remain are background events.

In order to "fake" a $\gamma\gamma$ event, two of the three photons from a $\pi^0\gamma$ event must take nearly all of the available energy, leaving one low energy photon which is undetected by the CCAL. Similarly from a $\pi^0\pi^0$ event which "fakes" a $\gamma\gamma$ event, two low energy photons are lost. In both cases, the two large energy photons which remain have essentially taken most of the energy and momentum of the parent pions; these feed-down events should therefore have an angular distribution which is essentially the same as that of the parent process.

The signal process, however, is expected to have a different angular distribution. Thus a cut on the polar angle θ of the γ candidates can help to maximize the signal-to-background ratio.

The $\pi^0\pi^0$ and $\pi^0\gamma$ cross sections and the feed-down backgrounds associated with them are sharply forward peaked. In Figs. 7.11 and 7.12 we show the $\pi^0\pi^0$ and $\pi^0\gamma$ cross sections in the η_c and η_c' regions, which demonstrate the forward peaking. In the figures we also present the $\gamma\gamma$ candidate events which have passed all cuts which we have discussed thus far. The angular distribution of those events roughly follows that of the $\pi^0\pi^0$ events as expected. We have chosen cut values of $|\cos(\theta^*)| \leq 0.2$ in the η_c region, and $|\cos(\theta^*)| \leq 0.4$ at higher energies $(\chi_J,\, \eta_c')$, where the forward peaking of the feed-down background begins. These cut values are indicated in Fig. 7.11 and 7.12.

The efficiency of this cut depends on our assumptions of the angular distribution of the process $\bar{p}p \to (c\bar{c})_R \to \gamma\gamma$. The pseudoscalar η_c must have an angular distribution which is isotropic, thus the acceptance of the cut in the η_c region is 0.2, for an ideal detector. Similarly, for a cut at $|\cos(\theta^*)| \leq 0.4$, which we make for η_c', (as well as the scalar χ_0) the acceptance is 0.4. As for the χ_2, since the $\bar{p}p \to \chi_2 \to \gamma\gamma$ process does not have an isotropic angular distribution, the acceptance of the cut at $|\cos(\theta^*)| \leq 0.4$ must be calculated carefully.

The analysis of the $\bar{p}p \to \chi_2 \to \gamma J/\psi$ reaction in E835 has shown that the χ_2 for-

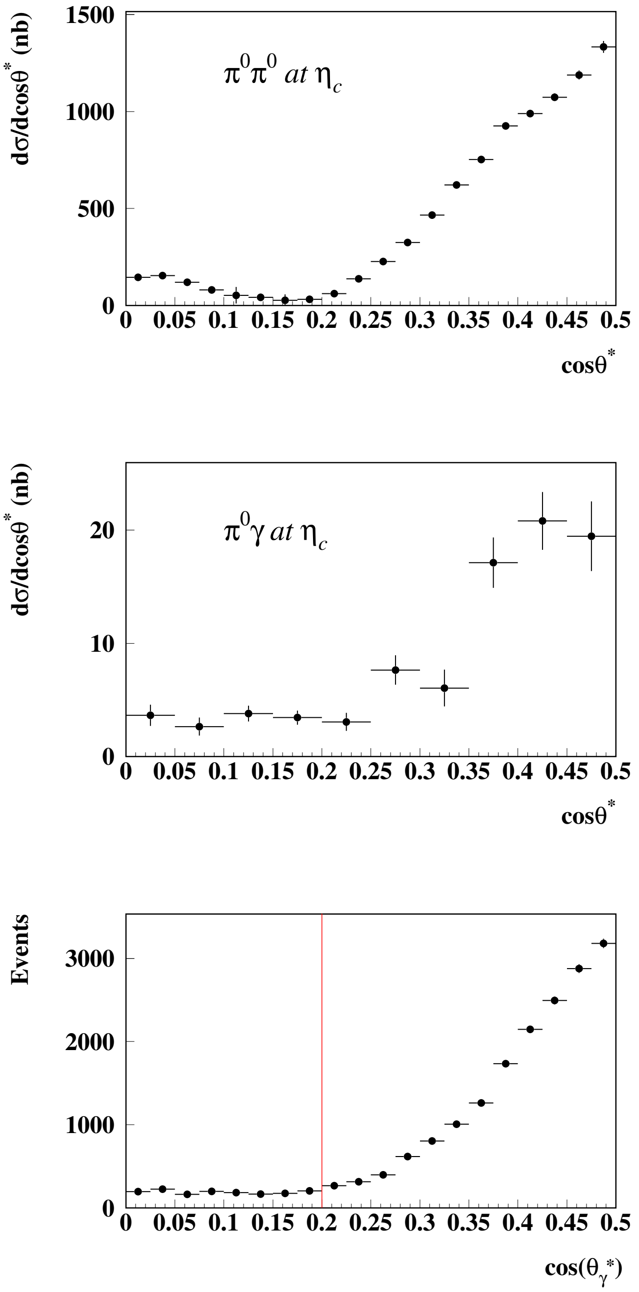

Figure 7.11: The top and middle panels show the measured $\pi^0\pi^0$ and $\pi^0\gamma$ angular distributions from E760 [51] at $\sqrt{s} = 2985$ MeV The bottom panel shows $\gamma\gamma$ candidate events from E835 (from the whole η_c region, 2911-3026 MeV) which satisfy all cuts discussed in this chapter.

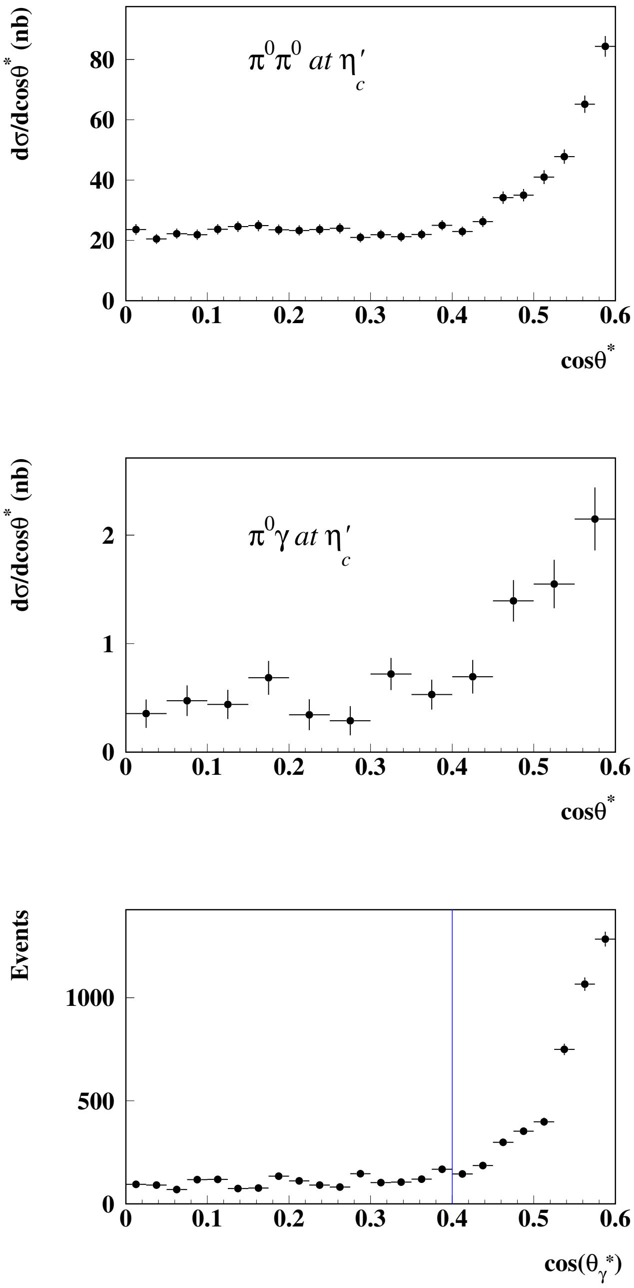

Figure 7.12: The top and middle panels show the measured $\pi^0\pi^0$ and $\pi^0\gamma$ angular distributions from E760 [51] at $\sqrt{s} = 3619$ MeV The bottom panel shows $\gamma\gamma$ candidate events from E835 (from the ${}^1P_1$ and η_c' regions, 3500 to 3660 MeV) which satisfy all cuts discussed in this chapter.

mation is dominated by the helicity 1 state of $\bar{p}p$. An upper limit (90% CL) of 26% was obtained for a possible helicity 0 component. [52] Further, it is theoretically predicted that in the $\chi_2 \rightarrow \gamma\gamma$ decay the helicity 2 component should dominate. The helicity 0 component of the $\chi_2 \rightarrow \gamma\gamma$ decay is predicted by models which take relativistic effects into account to be $\leq 5\%$ of the partial width. [53]

Pure helicity 1 formation followed by pure helicity 2 decay gives rise to an angular distribution of the form (see Ref. [48] for a derivation)

$$W(\theta^*) d\cos\theta^* = \frac{5}{4}[1 - \cos^4\theta^*] d\cos\theta^*.$$

Integration of the above function over our range of $\cos(\theta^*)$ from -0.4 to 0.4 gives an efficiency for $\chi_2 \rightarrow \gamma\gamma$ of 0.497, for an ideal detector.

Because of the fact that the efficiency of γ detection by the CCAL is not 100%, and may vary with time, we do not expect that the efficiencies for the polar angle cuts discussed above are exactly what we expect from geometrical considerations alone. We have therefore decided to evaluate the efficiency of the polar angle cuts by the Monte Carlo method described in the previous section.

7.2.6 Charged Track Contamination at J/ψ and ψ'

The kinematics of the reactions $\bar{p}p \rightarrow J/\psi \rightarrow e^+e^-$ and $\bar{p}p \rightarrow \gamma\gamma$ at $\sqrt{s} = M(J/\psi)$ are indistinguishable. The same is true for the two reactions at ψ'. Consequently, the events from $\bar{p}p \rightarrow (J/\psi, \psi') \rightarrow e^+e^-$ will pass all the cuts discussed in this chapter, unless the $\gamma\gamma$ trigger used removes them effectively.

We have analyzed events from the "gold gg" trigger set, and may therefore expect that the number of e^+e^- events in the initial data sample is very small. However, if the Neutral Veto were somehow inefficient at detecting (and rejecting) e^+e^- events, we would expect to find an excess of events which pass our cuts at the J/ψ and ψ' data points. Such a problem was discovered during the 1996 run, and as a result it is necessary to make an additional cut on charged tracks for the $\gamma\gamma$ trigger set for at least the J/ψ and ψ' stacks. For consistency, we have also decided to make the same cut for data taken at all energies.

The problem involves the neutral veto logic. "Holes" were found at azimuthal (ϕ) angles from $(23/24)\pi$ to π radians, and from $(47/24)\pi$ to 2π radians. (See Fig. 7.13) The detector elements involved were working correctly. However, the signal cables from the $H2'$ paddles in the two angular regions were not correctly connected to the neutral veto logic unit. As a result, $\bar{p}p \to e^+e^-$ events could pass the neutral two-body trigger in the regions of these holes. The unshaded histogram in Fig. 7.13 represents the azimuthal angle ϕ of each γ candidate in events which satisfy all the cuts mentioned above. The large excess of events near $\phi = \pi$ and $\phi = 2\pi$ indicates the above-mentioned "holes" in the Neutral Veto, through which $J/\psi \to e^+e^-$ events pass into the neutral trigger. In order to remove these events, we have made cuts on the pulse heights in hodoscopes $H1$ and $H2'$.

It is not unexpected that, δ-rays or random noise in the hodoscopes might cause a $\gamma\gamma$ event to register an pulse height of more than 0.5 MIPs in *one* of the four $H1$ and $H2'$ paddles through which the two photons pass. On the other hand, e^+e^- events can be expected to nearly always produce pulse heights of greater than 0.5 MIPs in at least three of the four paddles through which the electrons pass. For this reason, we remove events which have a pulse height of greater than 0.5 MIPs. in more than one of the four corresponding $H1$ or $H2'$ paddles.

The shaded histogram in Fig. 7.13 shows the events which are retained after the application of this cut on $H1$ and $H2'$. The excess near $\phi = 0$ and $\phi = \pi$ has beeen removed.

We have tested this cut for its ability to remove e^+e^- events from a clean J/ψ sample, and for its ability to retain clean $\pi^0\pi^0$ events, which is a test of its efficiency for our $\gamma\gamma$ event sample. From a clean sample of 5998 $J/\psi \to e^+e^-$ events taken from the J/ψ stacks used in the η_c analysis, a total of only 2 events remain after the application of the charged hodoscope cut - a 99.97% rejection factor. We have similarly studied 5.44 pb^{-1} of data taken in the ψ' region. There, we found no e^+e^- events which pass the analysis cuts, including the cut on $H1$ and $H2'$ described in this section.

The Poisson 90% confidence upper limit on 2 observed events is 5.91, and on 0 observed events, is 2.44. Therefore, at 90% confidence we expect fewer than $5.91 \times (1/24) = 0.25$ e^+e^- events in our sample of 22 $\gamma\gamma$ events at the J/ψ energy points due to the presence of the holes in the trigger. Similarly, we expect $(8.98/5.44) \times 2.44 \times 1/24 = 0.17$ events in our sample of 78 $\gamma\gamma$ events at the ψ' energy points. These contributions are completely negligible.

We have calculated the efficiency for $\gamma\gamma$ events using a clean sample of 9873 $\pi^0\pi^0$ events at η_c'. Of those, 9426 remain after the application of the $H1$ and $H2'$ cuts, leading to an efficiency of $95.47 \pm 0.21\%$.

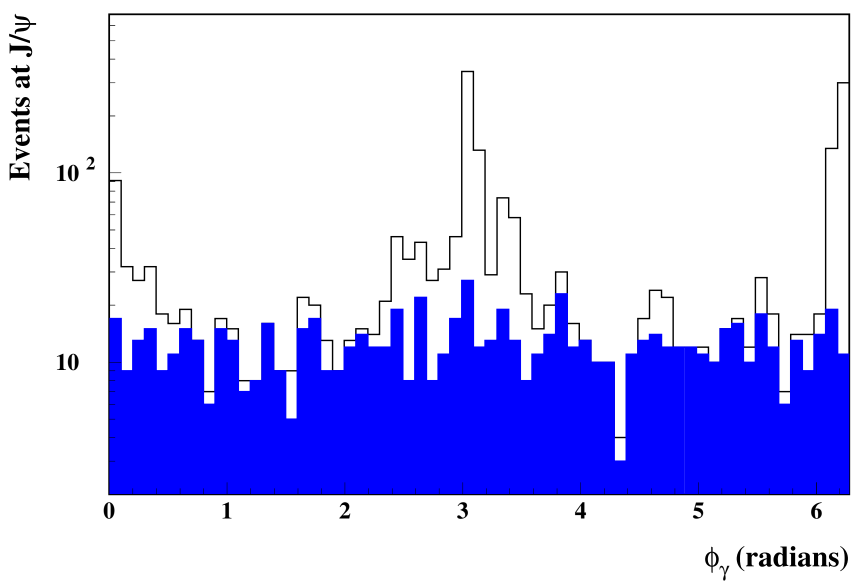

Figure 7.13: Azimuthal angle $\phi_{1,2}$ for neutral trigger events in the J/ψ stacks which satisfy all cuts described in the text. The unshaded histogram shows all such events; the peaks in the distribution at $\phi = 0$ and 2π show the effect of the trigger "holes". The shaded histogram represents the events which remain after application of the $H1$ and $H2'$ cuts described in the text.

7.3 Overall Efficiency of Cuts

The overall efficiency is determined by taking the product of the various efficiencies noted above, assuming their independence, and the $97.8\% = 1 - 2 \times 1.1\%$ beampipe conversion correction derived from Ref. [47]. With the stack-by-stack efficiency described in Sec. 7.2.2 denoted as ϵ_{MC}, the overall efficiency is $\epsilon = \epsilon_{MC} \times \alpha \times 0.934 \pm 0.020$. As mentioned above, this efficiency is calculated separately for each data point, and appears along with the summary of $\gamma\gamma$ data taken at all energy points in Table E.